INTERFACE FOCUS

rsfs.royalsocietypublishing.org

Review

Cite this article: Cox N, Pantazis DA, Neese F, Lubitz W. 2015 Artificial photosynthesis: understanding water splitting in nature. *Interface Focus* **5**: 20150009.
http://dx.doi.org/10.1098/rsfs.2015.0009

One contribution of 11 to a theme issue 'Do we need a global project on artificial photosynthesis (solar fuels and chemicals)?'.

Subject Areas:
chemical biology, bioenergetics, biophysics

Keywords:
photosynthesis, photosystem II, water splitting, H_2 production

Authors for correspondence:
Nicholas Cox
e-mail: nicholas.cox@cec.mpg.de
Wolfgang Lubitz
e-mail: wolfgang.lubitz@cec.mpg.de

THE ROYAL SOCIETY PUBLISHING

Artificial photosynthesis: understanding water splitting in nature

Nicholas Cox, Dimitrios A. Pantazis, Frank Neese and Wolfgang Lubitz

Max-Planck-Institut für Chemische Energiekonversion, Stiftstr. 34-36, 45470 Mülheim an der Ruhr, Germany

In the context of a global artificial photosynthesis (GAP) project, we review our current work on nature's water splitting catalyst. In a recent report (Cox *et al.* 2014 *Science* **345**, 804–808 (doi:10.1126/science.1254910)), we showed that the catalyst—a Mn_4O_5Ca cofactor—converts into an 'activated' form immediately prior to the O–O bond formation step. This activated state, which represents an all Mn^{IV} complex, is similar to the structure observed by X-ray crystallography but requires the coordination of an additional water molecule. Such a structure locates two oxygens, both derived from water, in close proximity, which probably come together to form the product O_2 molecule. We speculate that formation of the activated catalyst state requires inherent structural flexibility. These features represent new design criteria for the development of biomimetic and bioinspired model systems for water splitting catalysts using first-row transition metals with the aim of delivering globally deployable artificial photosynthesis technologies.

1. The need for a global project on artificial photosynthesis

The world's power supply is based predominantly on the use of non-renewable energy resources such as oil, coal and natural gas. These geological resources have been accumulated over millions of years from photosynthetic activity and thus constitute 'stored solar energy'. The steep rise in energy consumption over the last century has led to an inevitable shortage of these valuable resources with the economic, social and political consequences already felt today. Human population and economic growth, particularly in fast-developing countries, will lead to a further increase in energy demand. Furthermore, the burning of carbon-rich fuels has increased CO_2 concentration in the atmosphere. This increase is associated with anthropogenic climate changes, with projected adverse effects for our planet and human society (http://www.ipcc.ch/report). It is therefore one of the great challenges of mankind to identify and develop alternative sustainable energy sources [1–5].

Society's energy needs come in many forms. The dominant fraction is related to liquid fuels used for example in transportation (approx. 80%); whereas electrical energy only accounts for a small part of our energy consumption (approx. 20%) (https://www.bdew.de/internet.nsf/id/DE_Energiedaten). This is particularly problematic as there currently exists no satisfactory method which would be able to supply our demand for renewable liquid fuels. One possible solution would be to generate electricity using alternative, clean physical energy conversion technologies such as photovoltaics, wind turbines and hydropower and subsequently convert it into a chemical storage form. Such technologies already represent an increasing share of electrical energy generation worldwide (in Germany in 2013 16%) (https://www.bdew.de/internet.nsf/id/DE_Energiedaten). The question that then arises is what represents the best feedstock for a synthetic, renewable fuel. Here, biology provides an answer: photosynthesis uses water, a cheap, non-toxic, abundant material. Thus, in an idealized scenario 'clean' electricity would be used in the electrolysis of water, generating hydrogen (H_2), as a fuel [6]. Hydrogen itself is a very important base chemical and can be converted to many other important energy-rich materials for storage and/or transport, e.g. with CO_2 to methane, methanol or formic acid, and with molecular nitrogen to ammonia (figure 1).

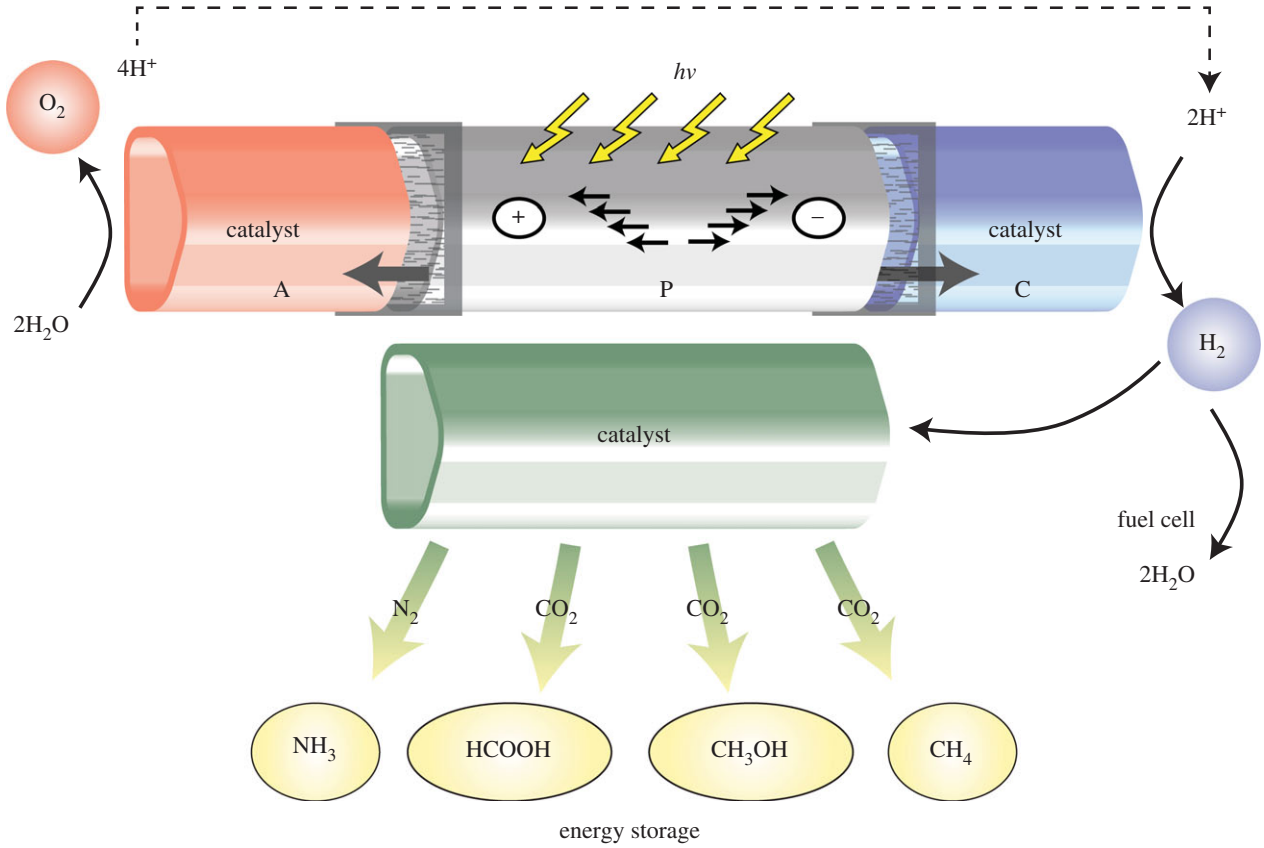

Figure 1. Biomimetic device showing light-induced charge separation in a photo(electro)catalyst P, transport of redox equivalents to a water splitting catalyst (A, anode) and to a hydrogen-producing catalyst (C, cathode). The generated primary 'solar fuel' is dihydrogen. This can be used directly, e.g. in fuel cells to generate electricity or burned in combustion engines, or can be converted for storage, transport or other uses. The examples are reactions with carbon dioxide to yield formic acid, methanol or methane and ammonia production with nitrogen (e.g. for fertilizers, agriculture). These reactions also require efficient catalysts.

A simple calculation shows that the yearly energy needs of a single person can be met by decomposition of 12 000 l of water, i.e. the contents of a small water pool ($4 \times 3 \times 1$ m). In addition, such a scenario eliminates the need for an independent power supplier, allowing energy production at the site of use [7], reducing transportation losses. A bottleneck though for such a 'hydrogen economy' blueprint is the relatively high price of the hydrogen produced. The high cost is derived from the materials used currently in commercially viable electrolysers: noble metals such as platinum or precious metal oxides (Ru and Ir oxides). These need to be replaced by less expensive metal catalysts before this model for the hydrogen economy becomes viable.

The generation of H_2 from water requires two catalytic steps: (i) the oxidation of two water molecules into O_2 and protons and (ii) the subsequent reduction of protons to molecular H_2. For proton reduction interesting approaches already exist (e.g. based on biomimetic catalysts from hydrogenase research) [8] that are close to enabling feasible commercial/industrial applications [9]. By contrast, there exists no completely satisfactory water oxidation catalyst. First-row transition metal based materials used for this reaction display typically a limited stability and durability (low turnover number, TON) or have an intrinsically low turnover frequency (TOF), precluding their wide range application. Another problem is often the excessive voltages needed to drive such catalysts (overpotential), which are due to the lack of suitable interfaces between the catalysts and the photo-active semiconductors.

Clearly renewed public investment should be targeted towards the scientific, technological and economic challenges needed to initiate the energy transition described above, e.g. the 'Energiewende' policy adopted by the current German government. The central discipline in this endeavour is *chemical catalysis* in all its facets, allowing energy to be efficiently used, stored, transported and interconverted. In this endeavour much can be learned from nature, which has developed many highly efficient metallo-enzymes [10] for the chemical conversion of small molecules with high TONs, long lifetimes and low overpotentials, and which even have built-in protection and repair mechanisms.

To solve the energy problems of the future requires initiatives such as the *Global Artificial Photosynthesis* (*GAP*) project [5], which bring together the efforts of many researchers across a wide range of scientific disciplines. Ideally, technologies that use nature as a blueprint, such as photosynthesis, should be considered part of the common heritage of mankind. We should aim that such technologies are affordable and accessible throughout the world with maximum benefit to all. We endorse the spirit of the *GAP* project: 'Our goal is to work cooperatively and with respect for basic ethical principles to produce the scientific breakthroughs that allow development and deployment of an affordable, equitably accessed, economically and environmentally sustainable, non-polluting global energy and food system that also contributes positively to our biosphere', as discussed at the Chicheley Hall conference in July 2014.

2. Design strategies for artificial photosynthesis, learning from nature

The term 'artificial photosynthesis' or equally 'synthetic photosynthesis' describes technologies that attempt to capture

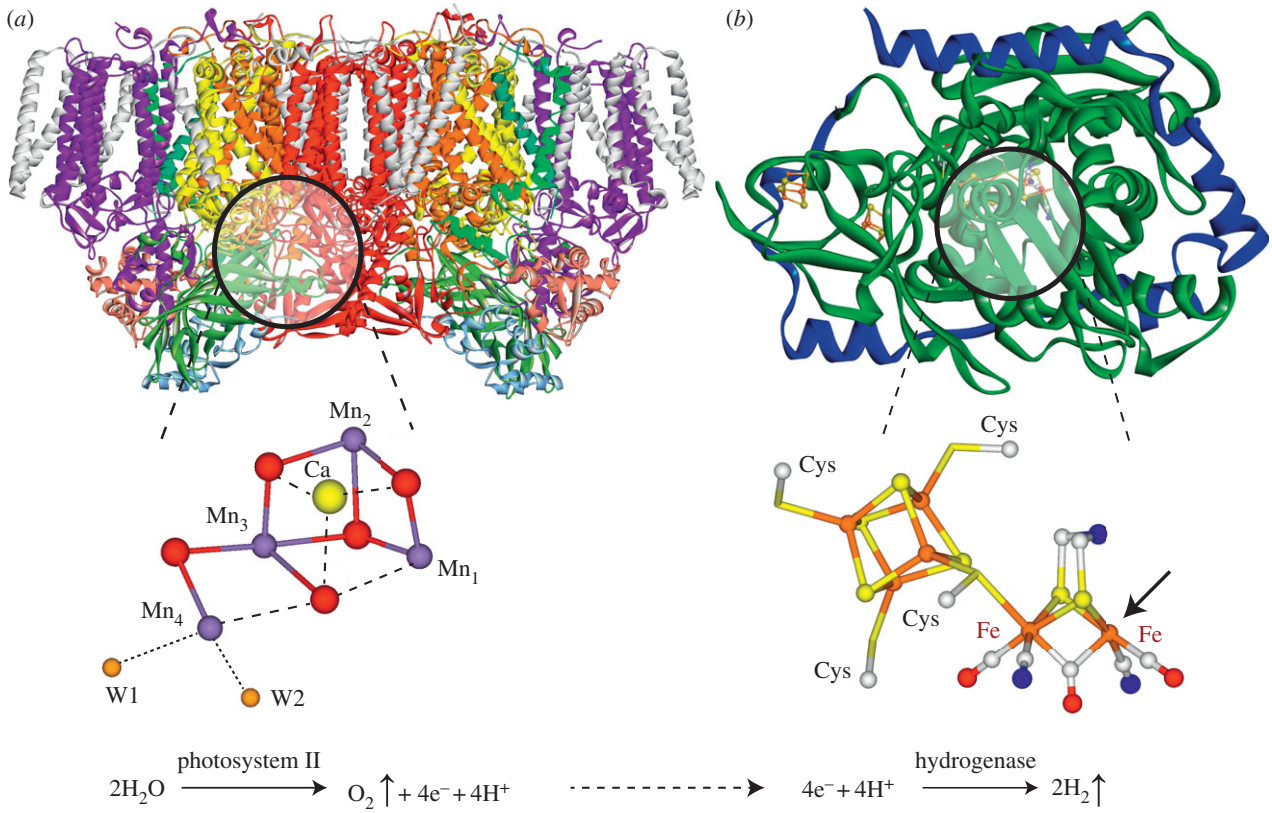

Figure 2. Light-induced water splitting into molecular oxygen and hydrogen by the enzymes PSII and [FeFe] hydrogenase. This cascade reaction (water oxidation and subsequent proton reduction) is for example exploited by green algae, e.g. *Chlamydomonas reinhardtii*. The structure of the proteins ((*a*) PDB 3ARC [11], (*b*) PDB 1HFE [12]) and the structure of the active sites are shown (see text for details).

the energy of sunlight to make energy-rich molecules, i.e. 'solar fuels'. This relies on the thesis that chemical bonds allow energy to be efficiently stored. This is essentially what nature does. It performs a photocatalytic water oxidation reaction which is coupled to carbon dioxide fixation (CO_2 reduction). In oxygenic photosynthesis, light-induced water oxidation occurs in a biological supercomplex, called photosystem II (PSII) that is found in all green plants, algae and cyanobacteria. It harbours a protein-embedded oxygen-bridged Mn_4Ca cluster with four bound water-derived ligands [11], as shown in figure 2. This cluster, called the water oxidizing complex (WOC) or oxygen evolving complex (OEC), is coupled to a pigment–protein reaction centre, which successively extracts electrons from it. After four such extractions, the complex splits water into protons and molecular oxygen, which is released as by-product, returning to its resting state (for reviews, see [13–16]). Protons generated via this process could, in principle, be used by another enzyme found in many green algae and bacteria, hydrogenase, which catalyses the conversion of protons to molecular hydrogen (for a recent review, see [8]). In figure 2 next to PSII, the structure of an [FeFe] hydrogenase is also depicted. The active site of this hydrogenase is a six-iron cluster, made up from a classical [4Fe–4S] cubane linked to a di-iron complex that carries uncommon ligands (3 CO, 2 CN^-, azadithiolate) [8]. Under certain metabolic conditions, this enzyme is activated and produces hydrogen from excess protons. Other types of hydrogenases are known that harbour a different binuclear metal cluster ([NiFe] hydrogenases) that converts H_2 into protons and electrons, thereby generating energy for the organism [8,17,18]. In principle, both types of hydrogenases catalyse both reactions, dihydrogen splitting and production, albeit with different rates.

The efficient coupling of these two biological processes, water oxidation and hydrogen production (shown in figure 2), is currently being investigated in many laboratories aiming at producing (bio)hydrogen [19–23]. An interesting feature of the enzymes is the high turnover rate, which is about 500 s^{-1} for the WOC and up to 10 000 s^{-1} for the hydrogenase [24]. Unfortunately, both enzymes suffer from limited stability: the WOC has a half-life of only 30 min in average light under working conditions [25] and the [FeFe] hydrogenase is very sensitive to oxygen [26,27]; in the living cell, protection and repair mechanisms exist that efficiently resynthesize and replace the damaged parts of the enzymes. Among the [NiFe] hydrogenases, there is also a class of oxygen-tolerant enzymes [28–32].

An understanding of the principles and mechanisms of water oxidation and hydrogen conversion in nature would allow us to better design artificial systems capable of (bio)hydrogen production, be they biological photosynthetic organisms or purely synthetic systems, such as the hypothetical device in figure 1. For this latter system, the ultimate aim is to synthesize new catalysts for large-scale water splitting, hydrogen production and energy storage in chemical compounds. Such compounds may also be of importance for a future sustainable energy economy. In this short review, the current knowledge about the enzyme water oxidase (PSII) is described as an example. It is not intended to describe in depth the biological system but instead focus on the active metal cluster, and the recent insight gained about its function by structural, spectroscopic and theoretical results. Design criteria for the construction of respective biomimetic and bioinspired model systems for water splitting are discussed. We note that the reversible conversion of protons to molecular hydrogen is described in recent reviews (e.g. [8]).

3. Nature's water splitting catalyst

Nature's water oxidizing catalyst represents a penta-oxygen tetramanganese–calcium cofactor (Mn_4O_5Ca) [11,13,16] (figure 2). Its catalytic cycle comprises five distinct redox intermediates, the S_n states, where the subscript indicates the number of stored oxidizing equivalents ($n = 0$–4) required to oxidize two water molecules and release dioxygen [33] (figure 3*b*). It is embedded in a unique pigment–protein supercomplex, PSII, which acts as a photosensitizer. Outer light harvesting complexes absorb visible light and funnel excitation energy to the reaction centre of PSII, where charge separation takes place. The reaction centre comprises chlorophyll, pheophytin and quinone molecules arranged about a twofold symmetry axis [35]. The radical cation generated upon charge separation, termed the primary oxidant ($P680^{\bullet+}$), is predominately associated with the chlorophylls P_{D1} and P_{D2} (figure 3*a*). The photochemically generated electron is passed in succession to the pheophytin ($Pheo_{D1}$) and subsequently to the bound plastoquinone (Q_A), increasing the electron–hole distance, thus stabilizing the charge separated state. Reaction centre photochemistry occurs on a picosecond to nanosecond time scale [35].

Subsequently, the electron is passed from Q_A to a second plastoquinone (Q_B), which acts as a mobile charge carrier. It accepts two electrons and two protons, before leaving its protein pocket to be exchanged with a new plastoquinone. In this way, electrons are passed to the next photosynthetic supercomplex, the cytochrome b_6f complex.

The photogenerated cation $P680^{\bullet+}$ is coupled to the Mn_4O_5Ca cofactor via an intermediary redox-active tyrosine residue Y_Z, which acts as a single-electron gate (figure 3*a*). Initial electron (hole) transfer between $P680^{\bullet+}$ and Y_Z occurs on a nanosecond time scale, whereas the subsequent electron (hole) transfer between $Y_Z^{\bullet}$ and the Mn_4O_5Ca cofactor occurs on a microsecond to millisecond time scale, depending on the intermediate (S-state). Fast reversible oxidation of Y_Z is a property of the protein pocket. A nearby histidine residue acts as an intermolecular base, stabilizing the deprotonated (Tyr-O$^{\bullet}$) state, while structured waters (bound to the Ca^{2+} ion) act to tune its redox potential [11,36]. After four charge separation events, the transiently formed $S_3Y_Z^{\bullet}$ state [S_4] rapidly decays to the S_0 state with the concomitant release of molecular triplet dioxygen and probably the rebinding of one substrate water molecule [37,38].

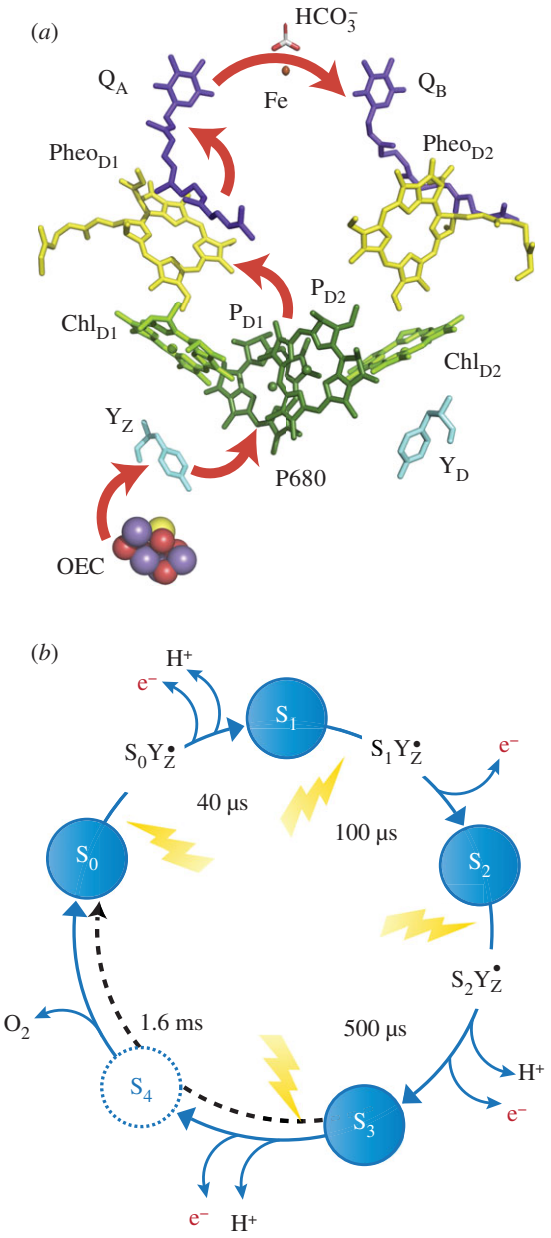

Figure 3. (*a*) Electron transport chain of PSII linking reaction centre photochemistry to the site of water splitting catalysis. (*b*) The catalytic (Kok) [33] cycle of the cofactor showing the sequence of electron and proton withdrawals and the time constant for each transition [34].

4. Key design features of the oxygen evolving complex

Nature's 'photosynthetic cell'—the water splitting cofactor coupled to the pigment–protein reaction centre photosynthesizer—has a number of unique design features, including the following.

(i) Light-induced single-electron transfer on a picosecond time scale coupled to a much slower millisecond four-electron process, the oxidation of two water molecules to molecular oxygen.

(ii) The temporary storage of oxidation equivalents required for this reaction, i.e. transient oxidation of the Mn ions.

(iii) Decoupling of O–O bond formation and proton release. Protons are released continuously throughout the S-state cycle [34], whereas the O–O bond forms in a single concerted step. Cofactor oxidation coupled with deprotonation (charge balancing/redox levelling) ensures that the redox potential of each of the four-electron withdrawal steps is similar, allowing all transitions to be driven by a single oxidant, P680, i.e. it lowers the overpotential needed to drive catalysis.

(iv) Efficient interfacing of the catalyst and the photosensitizer via a redox-active tyrosine Yz.

(v) Regulated substrate (water) delivery and product release (O_2, H^+) via protein channels.

(vi) Protection and repair mechanisms that limit oxidative damage of the protein pocket and replace the protein scaffold every 30 min under full sunlight [39]. It is noted that the water splitting catalyst binds to the protein and assembles spontaneously from free Mn^{2+} and Ca^{2+} in solution under visible light, a process called photoactivation [40].

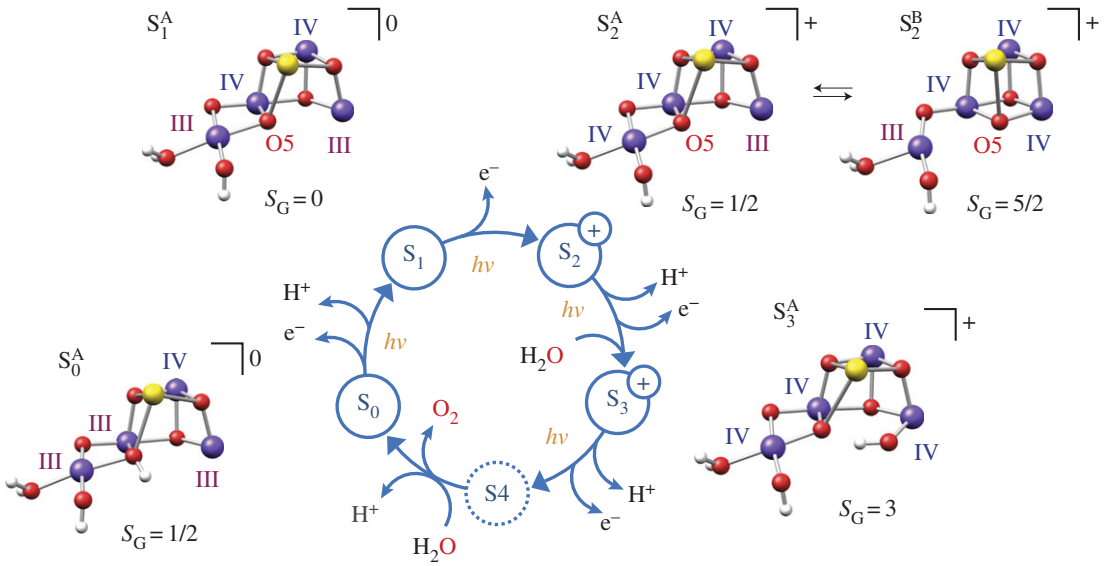

Figure 4. Models for each S state of the Kok cycle, showing the optimized geometry, protonation pattern and Mn oxidation states of the inorganic core, modified from Krewald *et al.* [55]. The cofactor exists in two forms in the S_2 state, an open cubane (S_2^A, $S_G = 1/2$) and a closed cubane (S_2^B, $S_G = 5/2$) structure which differ in their core connectivity by the reorganization of O5 [52].

5. The structure of the catalyst

The arrangement of the five metal ions and the connectivity of the cofactor (oxo bridges) have been resolved by conventional X-ray crystallography using synchrotron radiation (XRD) [11] supplemented by femtosecond X-ray crystallography using a free electron laser (XFEL) [41]. The structure represents a distorted chair where the back of the chair is defined by a plane containing Mn_1, Mn_3 and Mn_4. A second plane containing the Ca ion and Mn_2 defines the front of the chair. The Mn–Mn distances seen in the XRD structure are systematically longer than those seen in extended X-ray absorption fine structure (EXAFS) and in model complexes [42–46]. This is not the case for the XFEL structure, where the same Mn–Mn distances as seen in EXAFS are observed. The longer Mn–Mn distances in the XRD structure are thought to reflect reduction [47–49] of the Mn ions, and as such the XFEL structure is considered more reliable.

Our own work has concentrated on the development of methods for calculation of spectroscopic observables from magnetic resonance and X-ray spectroscopies, to further refine structural models of the cofactor and precisely describe the electronic structure of the catalyst in all catalytic states [50,51]. Our starting point was the structure of the cofactor in the S_2 state, for which extensive spectroscopic data exist, in which the net oxidation state of the cofactor is $Mn^{III}Mn_3^{IV}$. Theoretical modelling has shown that the cofactor can adopt two interconvertible core topologies in this state [52–54], an open cubane (S_2^A) and a closed cubane motif (S_2^B) (figure 4). The S_2^A form is slightly lower in energy by *ca* 1 kcal mol^{-1} and displays an electronic ground state of spin $S_G = 1/2$. In this structure, the only Mn^{III} ion of the cofactor, which is five-coordinate, is found within the cuboidal unit (Mn1, figure 5*a*). In the S_2^B form, the cofactor instead displays an electronic ground state of spin $S_G = 5/2$. In this structure, the five-coordinate Mn^{III} ion is now located at the terminal Mn4 (figure 5*a*) [52–54]. Movement of the Mn^{III} site is thus coupled to a reorganization of the core connectivity of the cofactor, involving the movement of a single μ-oxo bridge (O5) (figures 4 and 5*a*). In the open structure (S_2^A), O5 represents a bis-μ-oxo linkage between Mn3 and Mn4 (open form, S_2^A), whereas in the closed structure it becomes (S_2^A) a vertex of the heterobimetallic cubane unit. These two structures show a one-to-one correspondence with the two well-known electron paramagnetic resonance (EPR) signals for the S_2 state, the multiline ($S = 1/2$) and g4 ($S = 5/2$) signals (figure 5*a*) [52].

Recent multifrequency EPR measurements from our laboratory have now resolved the net oxidation state of the S_3 state (figure 5*b*). We find the net oxidation state of the cofactor is Mn_4^{IV} [56], categorically ruling out a ligand centred oxidation during the S_2–S_3 transition as has been proposed in the literature. Concomitant double resonance data suggest that the cofactor adopts a single configuration (unlike the S_2 state), which is best described as an open cubane (S_3^A) structure (figures 4 and 5*b*). Importantly, these results require that all four Mn ions are six coordinate in the S_3 state. This constraint necessitates the binding of a new water molecule to the open coordination site of the cofactor in the form of a hydroxide (figures 4 and 5*b*) [56,59]. Further evidence for water binding during the S_2–S_3 transition comes from work of the Noguchi laboratory [60]; their Fourier transform infrared spectroscopic data suggest that the solvation of the cluster increases during the S_2–S_3 transition. Interpretations of X-ray absorption near-edge structure data of the S_2–S_3 state are also consistent with a water binding event, where the absence of a large edge shift may reflect the five-coordinate Mn^{III} ion of the S_2 state becoming six coordinate in the S_3 state [61].

From this starting point, i.e. an understanding of the atomic structure of the S_2 and S_3 states that includes assignments of the energetically most favourable and spectroscopically consistent protonation states of all titratable ligands [55], we recently extended our spectroscopy-oriented theoretical modelling to the S_0 and S_1 states. The guiding principle for selecting the best models was again maximal consistency with experimental observables, including spin states ($S_G = 1/2$ for S_0 and $S_G = 0$ for S_1) [56,62,63], Mn hyperfine couplings, metal–metal distances from EXAFS and profiles of Mn K-pre-edge X-ray absorption spectra [55]. Figure 4 summarizes the results of this effort, showing the cofactor geometry, protonation states of titratable groups and individual Mn oxidation states for all spectroscopically consistent S-states models of the Kok cycle.

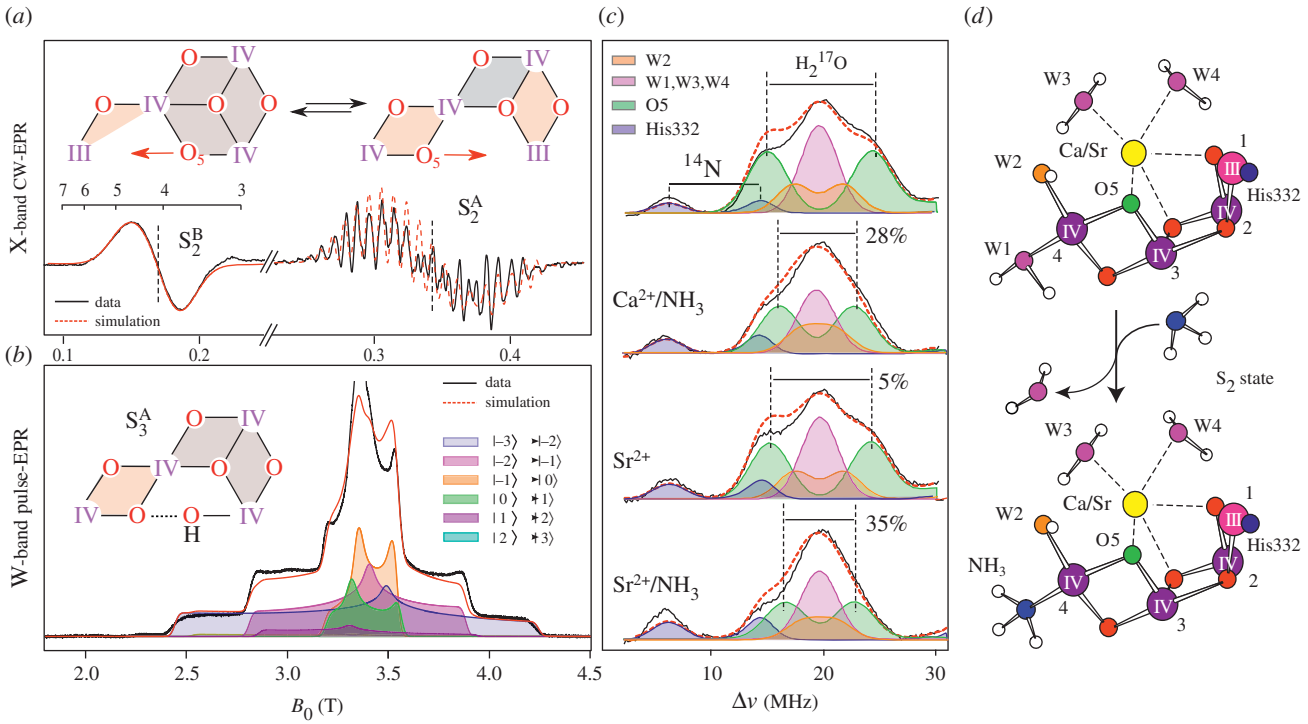

Figure 5. (*a*) CW-EPR data of the two forms of the S_2 state (S_2^A and S_2^B) modified from Cox *et al*. [13]. (*b*) High field (W-band) data of the S_3 state consistent with an open S_3^A type structure, modified from Cox *et al*. [56]. (*c*) ^{17}O-EDNMR data of exchangeable oxygen sites of the Mn_4O_5Ca cofactor, modified from Lohmiller *et al*. [57]. The splitting of the largest doublet (green, O5) is sensitive to both Ca^{2+}/Sr^{2+} replacement and W1/NH_3 exchange. (*d*) Replacement of W1 by NH_3. Also shown are the three different sites where ^{17}O labelled water is taken up by the cofactor: (i) as a ligand to the Ca^{2+} ion, (ii) as a ligand to the outer Mn4 ion and (iii) as a μ-oxo bridge (O5) [58].

6. The substrate (water) molecules of the oxygen evolving complex

Experiments performed with isotopically labelled water ($H_2^{17}O$/ $H_2^{18}O$) provide a means to identify the two substrate binding sites of the water oxidizing cofactor. Earlier membrane-inlet mass spectrometry (MIMS) results [64], which monitor the uptake of $H_2^{18}O$ into the product O_2 molecule, have demonstrated that the complex contains two chemically different substrate sites: an early (W_s) and late (W_f) binding substrate site, both of which exchange with bulk water in all catalytic states (S-states) [65–67]. Owing to the relatively slow rate of exchange of W_s (≈1 s^{-1}), and its dependence on the oxidation state of the Mn tetramer, W_s is usually considered to be an oxygen ligand of one of the Mn ions [38,67]. By using water labelled with the magnetic isotope (^{17}O, $I = 5/2$), the same substrate binding site (W_s) can be characterized spectroscopically, using the EPR technique ELDOR-detected NMR (EDNMR) [13,58,68]. These measurements identify a unique, exchangeable μ-oxo bridge as a potential candidate for W_s and the identity of the exchangeable μ-oxo bridge has been inferred from small site perturbations of the cofactor (figure 5*c*).

Ammonia, a substrate water analogue, is known to bind to the water oxidizing cofactor in the S_2 state [69,70]. Its binding mode was recently determined as a terminal ligand to the Mn4 ion, replacing the water ligand W1 [71,72]. Such a binding motif readily explains the observed hyperfine and quadrupole couplings; the asymmetric quadrupole coupling is a property of the H-bonding network of the W1/NH_3 site (Asp61) [57,72]. W1 displacement as opposed to other binding modes (μ-oxo bridge displacement) is also preferred based on energetic considerations and an analysis of available vibrational data [71–73]. In samples where NH_3 is added, the hyperfine coupling of the exchangeable μ-oxo bridge is strongly perturbed (*ca* 30%) [57,72]. This result is readily understood as due to a *trans* effect: the W1 ligand is *trans* to the O5 bridge. Displacement of W1 by NH_3 elongates the O5–Mn4 distance perturbing the observed hyperfine coupling (figure 5*c*,*d*) [71].

The assignment that the exchangeable μ-oxo bridge is O5 is further supported by measurements on PSII, where the Ca^{2+} ion is biosynthetically replaced with Sr^{2+} [57]. In such samples, the hyperfine coupling of the exchangeable μ-oxo bridge is perturbed (*ca* 5%, figure 5*c*). As O5 is a ligand to the Ca^{2+}/Sr^{2+} site this result is again easily understood. Furthermore, in samples where the Ca^{2+} is replaced by Sr^{2+} ***and*** NH_3 is bound to the cofactor, an ***additive*** effect is seen on the exchangeable μ-oxo bridge hyperfine coupling (*ca* 35%) [57], again consistent with the notion that O5 represents the exchangeable μ-oxo bridge (figure 5*c*).

The above results on Ca^{2+}/Sr^{2+} exchange point to O5 representing W_s. This hypothesis comes from correlation to MIMS results which show that Ca^{2+}/Sr^{2+} replacement perturbs the rate at which W_s exchanges with bulk water [38,67,74]. As Ca^{2+}/Sr^{2+} replacement similarly affects the electronic properties of O5 (but no other exchangeable oxygen ligand) [57], this result can again be easily understood. We note that the fast rate of exchange of O5 when compared with that of μ-oxo bridges in simple synthetic model systems is likely due to the unusual flexibility of its metal coordination (figures 4–6) [52,53].

Assignment of the second substrate site W_f is less clear. The above description of the structure of the S_3 state suggests that the second substrate would represent the newly bound terminal hydroxide ligand, in close proximity to O5/W_s.

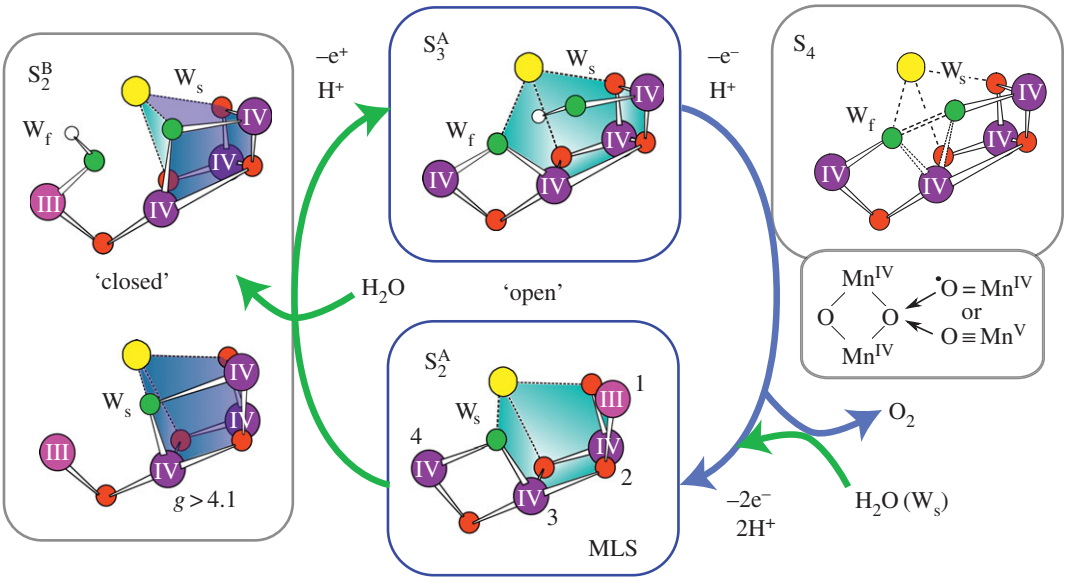

Figure 6. The reaction cycle of the Mn_4O_5Ca cofactor. In the resting states (S_0, S_1, S_2^A), the cofactor represents an 'open' cubane structure with an open coordination site for substrate binding. In the activated states (S_3 and possibly S_4), the structure also resembles an 'open' cubane but now the open coordination site is occupied by a hydroxide ligand. Structural flexibility in S_2 (S_2^A, S_2^B) is hypothesized to be critical for the insertion of this water-derived ligand and formation of an activated S_3 state. The O–O bond may then presumably form between the flexible μ-oxo bridge and the inserted (proximal) water-derived ligand.

This result though appears at odds with MIMS data that show that W_f's exchange kinetics are almost identical for the S_2 and S_3 states [13,37,75], suggesting that it is associated with the Mn_4O_5Ca cofactor in the S_2 and S_3 states in the same way [38,75]. A possible solution is that W_f represents a pre-existing water ligand of the cluster (W2 bound to the Mn4 ion or W3 bound to Ca^{2+} ion) which is relocated in the S_3 state, suggesting a concerted mechanism for substrate delivery [38,71,75,76].

7. The reaction cycle of the catalyst

As described above, the water oxidizing cofactor takes two discrete conformations during its catalytic cycle and as such, its reaction cycle can be divided into two (figure 6). In the 'resting' S-states (S_0, S_1), the cofactor adopts a low-spin configuration ($S = 1/2$ and 0) [62,63]. Calculations demonstrate that this is a property of the incomplete cuboidal unit [52,55], i.e. a manganese unit with a vacant coordination site. In this form, the catalyst is inactivated. In the 'activated' S states, the cofactor instead adopts a high-spin configuration ($S = 3$) [56], concomitant with the insertion of a water ligand into the cubodial unit. S_2 displays both low- and high-spin forms ($S = 1/2$ for the open cubane form S_2^A, $S = 5/2$ for the closed cubane form S_2^B) suggesting that it may represent a switching point in the catalytic cycle (figure 6). Spin-state interconversion, which involves the opening of the cubodial unit may facilitate water insertion/relocation into the hetero-bimetallic cubane. It is noted that EPR data suggest that Ca^{2+} is necessary to proceed past the low-spin $S_2Y_Z^{\bullet}$ state, and thus Ca^{2+} may play a role either in allowing efficient S_2^A/S_2^B interconversion, or at least in allowing spin-state crossover [77–79]. It is then the high-spin topology that allows low barrier single-product formation to proceed, for example, via an oxo–oxyl coupling mechanism as proposed by Siegbahn [56,59,80]. Late second substrate binding may avoid deleterious two-electron chemistry (slow peroxide formation) in the resting states of the catalytic cycle [81].

8. Conclusion and outlook

The results described above place new, important restrictions on the structure of nature's water oxidizing cofactor, its catalytic cycle and the mechanism of water splitting and O_2 evolution. These are listed below with reference to design criteria for the development of biomimetic and bioinspired water splitting catalysts using manganese.

(i) The oxidation states of all individual Mn sites in all S-states are now resolved: S_0 $(Mn^{III})_3Mn^{IV}$, S_1 $(Mn^{III})_2(Mn^{IV})_2$, S_2 $Mn^{III}(Mn^{IV})_3$, S_3 $(Mn^{IV})_4$ and ligand oxidation can be excluded prior to formation of the S_4 state. This assignment is in agreement with the average Mn oxidation state inferred for heterogeneous manganese oxide water oxidation catalysts [82].

(ii) An exchangeable μ-oxo bridge (O5) is likely the first substrate of the water splitting reaction. This result, coupled with the observation that the cofactor gains a new hydroxide ligand in the S_3 state supports the notion that the O–O bond forms between oxygen ligands of neighbouring redox-active Mn ions (Mn_1 and Mn_4).

(iii) Structural flexibility of the cofactor appears to be critical for function, namely catalyst activation, i.e. the formation of the S_3 state, which is coupled to second substrate inclusion. This flexibility is only readily apparent in the S_2 state, with the other S-states adopting a single preferred configuration. This property seems to be conferred in part by the Ca^{2+} ion, which also may act to tune the redox/magnetic properties of the cuboidal (Mn_3Ca) unit [83], or of the tyrosine radical [36] or both. The inclusion of calcium has been correlated with enhanced water splitting activity of manganese oxide water oxidation catalysts [82,84].

The heterobimetallic nature of the cluster and the choice of Mn as the redox active metal for biological water

splitting must therefore reflect a confluence of effects. Key properties are

(i) that it can stabilize multiple oxidation states to be accessed over a narrow range of redox potentials. This property is derived from protein/cofactor interactions being able to tune the pK_a of cofactor bound water (substrate) molecules allowing sequential H^+ release upon each Mn oxidation event;
(ii) the possibility that the heterobimetallic cubane allows the formation of an energetically accessible Mn^V-oxo or Mn^{IV}-oxyl radical in the transition state [85–88]; and
(iii) that the Mn ions represent trapped valence states of local high-spin states, which magnetically couple together in a precise way in each S-state.

While the points above pose interesting theoretical questions, from a more practical perspective, the static properties of heterobimetallic cubane appear to be universal and can be reproduced in simpler model compound systems [89–91]. Similarly, heterogeneous Mn/Ca materials already show reasonable, if somewhat slow water splitting capacity normalized to Mn content [82,92,93]. Although it cannot be excluded that such Mn/Ca materials adopt lower efficiency pathways for O–O bond formation, the alternative explanation, that such materials only contain an intrinsically small number of 'active' heterobimetallic cubane units, seems equally reasonable. If, as figure 6 suggests, nature's catalyst essentially toggles between an 'inactive' and 'active' form, the latter having a substrate bound within the heterobimetallic cubane, the challenge in designing a better catalyst amounts to introducing this property (structural flexibility) or stabilizing a solvent accessible cuboidal structure that is stable/robust. These key design criteria should form the basis for new synthetic complex development—akin to the progress recently made in H_2 production using hydrogenase mimics [9]—for water splitting catalysts using manganese.

Acknowledgements. We thank Dr Alain Boussac (Saclay, France) and Prof. Johannes Messinger (Umea, Sweden) for helpful discussions.
Funding statement. This work was supported by the MPG, the Cluster of Excellence RESOLV (EXC 1069) and the DIP (Lu 315/17-1), both funded by the Deutsche Forschungsgemeinschaft (DFG).

References

1. Wydrzynski TJ, Hillier W (eds). 2012 *Molecular solar fuels*. Cambridge, UK: RSC Publishing.
2. Schlögl R (ed.). 2013 *Chemical energy storage*. Berlin, Germany: Walter de Gruyter GmbH.
3. Olah GA, Goeppert A, Prakash GKS. 2006 *Beyond oil and gas: the methanol economy*. Weinheim, Germany: Wiley-VCH.
4. Faunce TA. 2011 Future perspectives on solar fuels. In *Molecular solar fuels* (eds TJ Wydrzynski, W Hillier), pp. 506–528. Cambridge, UK: RSC Publishing.
5. Faunce TA *et al*. 2013 Energy and environment policy case for a global project on artificial photosynthesis. *Energy Environ. Sci.* **6**, 695–698. (doi:10.1039/c3ee00063j)
6. Rand DAJ, Dell RM. 2008 *Hydrogen energy. Challenges and prospects*. Cambridge, UK: RSC Publishing.
7. Nocera DG. 2012 The artificial leaf. *Acc. Chem. Res.* **45**, 767–776. (doi:10.1021/ar2003013)
8. Lubitz W, Ogata H, Rüdiger O, Reijerse E. 2014 Hydrogenases. *Chem. Rev.* **114**, 4081–4148. (doi:10.1021/cr4005814)
9. Simmons TR, Berggren G, Bacchi M, Fontecave M, Artero V. 2014 Mimicking hydrogenases: from biomimetics to artificial enzymes. *Coordin. Chem. Rev.* **270**, 127–150. (doi:10.1016/j.ccr.2013.12.018)
10. Holm RH, Solomon EI (eds). 2014 Special issue on *Bioinorganic enzymology II. Chem. Rev*. **114 (7,8)**.
11. Umena Y, Kawakami K, Shen J-R, Kamiya N. 2011 Crystal structure of oxygen-evolving photosystem II at a resolution of 1.9Å. *Nature* **473**, 55–60. (doi:10.1038/nature09913)
12. Nicolet Y, Piras C, Legrand P, Hatchikian CE, Fontecilla-Camps JC. 1999 *Desulfovibrio desulfuricans* iron hydrogenase: the structure shows unusual coordination to an active site Fe binuclear center. *Structure* **7**, 13–23. (doi:10.1016/S0969-2126(99)80005-7)
13. Cox N, Pantazis DA, Neese F, Lubitz W. 2013 Biological water oxidation. *Acc. Chem. Res.* **46**, 1588–1596. (doi:10.1021/ar3003249)
14. McEvoy JP, Brudvig GW. 2006 Water-splitting chemistry of photosystem II. *Chem. Rev.* **106**, 4455–4483. (doi:10.1021/cr0204294)
15. Renger G (ed.). 2008 *Primary processes of photosynthesis—part 2. Principles and apparatus*. Cambridge, UK: RSC Publishing.
16. Yano J, Yachandra V. 2014 Mn_4Ca cluster in photosynthesis: where and how water is oxidized to dioxygen. *Chem. Rev.* **114**, 4175–4205. (doi:10.1021/cr4004874)
17. Pandelia ME, Ogata H, Lubitz W. 2010 Intermediates in the catalytic cycle of [NiFe] hydrogenase: functional spectroscopy of the active site. *Chem. Phys. Chem.* **11**, 1127–1140. (doi:10.1002/cphc.200900950)
18. Shafaat HS, Rüdiger O, Ogata H, Lubitz W. 2013 [NiFe] hydrogenases: a common active site for hydrogen metabolism under diverse conditions. *Biochim. Biophys. Acta* **1827**, 986–1002. (doi:10.1016/j.bbabio.2013.01.015)
19. Cammack R. 2011 The catalytic machinery. In *Hydrogen as a fuel: learning from nature* (eds R Cammack, M Frey, R Robson), pp. 159–180. London, UK: Taylor & Francis.
20. Gaffron H, Rubin J. 1942 Fermentative and photochemical production of hydrogen in green algae. *Gen. Physiol.* **26**, 219–240.
21. Ghirardi ML, Dubini A, Yu J, Maness P-C. 2009 Photobiological hydrogen-producing systems. *Chem. Soc. Rev.* **38**, 52–61. (doi:10.1039/B718939G)
22. Kruse O, Hankamer B. 2010 Microalgal hydrogen production. *Curr. Opin. Biotechnol.* **21**, 238–243. (doi:10.1016/j.copbio.2010.03.012)
23. Melis A, Happe T. 2001 Hydrogen production. Green algae as a source of energy. *Plant Physiol.* **127**, 740–748. (doi:10.1104/pp.010498)
24. Madden C, Vaughn MD, Diez-Perez I, Brown KA, King PW, Gust D, Moore AL, Moore TA. 2012 Catalytic turnover of [FeFe]-hydrogenase based on single-molecule imaging. *J. Am. Chem. Soc.* **134**, 1577–1582. (doi:10.1021/ja207461t)
25. Ohad I, Kyle DJ, Arntzen CJ. 1984 Membrane protein damage and repair: removal and replacement of inactivated 32-kilodalton polypeptides in chloroplast membranes. *J. Cell Biol.* **99**, 481–485. (doi:10.1083/jcb.99.2.481)
26. Swanson KD *et al*. 2015 [FeFe]-hydrogenase oxygen inactivation is initiated at the H cluster 2Fe subcluster. *J. Am. Chem. Soc*. **137**, 1809–1816. (doi:10.1021/ja510169s)
27. Vincent KA, Parkin A, Lenz O, Albracht SPJ, Fontecilla-Camps JC, Cammack R, Friedrich B, Armstrong FA. 2005 Electrochemical definitions of O_2 sensitivity and oxidative inactivation in hydrogenases. *J. Am. Chem. Soc.* **127**, 18 179–18 189. (doi:10.1021/ja055160v)
28. Pandelia ME, Lubitz W, Nitschke W. 2012 Evolution and diversification of Group 1 [NiFe] hydrogenases. Is there a phylogenetic marker for O_2-tolerance? *Biochim. Biophys. Acta* **1817**, 1565–1575. (doi:10.1016/j.bbabio.2012.04.012)
29. Pandelia ME, Nitschke W, Infossi P, Giudici-Orticoni MT, Bill E, Lubitz W. 2011 Characterization of a unique [FeS] cluster in the electron transfer chain of

the oxygen tolerant [NiFe] hydrogenase from *Aquifex aeolicus*. *Proc. Natl Acad. Sci. USA* **108**, 6097–6102. (doi:10.1073/pnas.1100610108)

30. Shomura Y, Yoon K-S, Nishihara H, Higuchi Y. 2011 Structural basis for a [4Fe-3S] cluster in the oxygen-tolerant membrane-bound [NiFe]-hydrogenase. *Nature* **479**, 253–257. (doi:10.1038/nature10504)
31. Fritsch J, Scheerer P, Frielingsdorf S, Kroschinsky S, Friedrich B, Lenz O, Spahn CMT. 2011 The crystal structure of an oxygen-tolerant hydrogenase uncovers a novel iron–sulphur centre. *Nature* **479**, 249–252. (doi:10.1038/nature10505)
32. Wulff P, Day CC, Sargent F, Armstrong FA. 2014 How oxygen reacts with oxygen-tolerant respiratory [NiFe]-hydrogenases. *Proc. Natl Acad. Sci. USA* **111**, 6606–6611. (doi:10.1073/pnas.1322393111)
33. Kok B, Forbush B, McGloin M. 1970 Cooperation of charges in photosynthetic O_2 evolution—I. A linear four step mechanism. *Photochem. Photobiol.* **11**, 457–467. (doi:10.1111/j.1751-1097.1970.tb06017.x)
34. Klauss A, Haumann M, Dau H. 2012 Alternating electron and proton transfer steps in photosynthetic water oxidation. *Proc. Natl Acad. Sci. USA* **109**, 16 035–16 040. (doi:10.1073/pnas.1206266109)
35. Cardona T, Sedoud A, Cox N, Rutherford AW. 2012 Charge separation in photosystem II: a comparative and evolutionary overview. *Biochim. Biophys. Acta* **1817**, 26–43. (doi:10.1016/j.bbabio.2011.07.012)
36. Retegan M, Cox N, Lubitz W, Neese F, Pantazis D. 2014 The first tyrosyl radical intermediate formed in the S2–S3 transition of photosystem II. *Phys. Chem. Chem. Phys.* **16**, 11 901–11 910. (doi:10.1039/c4cp00696h)
37. Hillier W, Messinger J. 2005 Mechanism of photosynthetic oxygen production. In *Photosystem II: the light-driven water:plastoquinone oxidoreductase* (eds T Wydrzynski, K Satoh), pp. 567–608. In series *Advances in photosynthesis and respiration*, vol. 22 (ed. Govindjee). Dordrecht, The Netherlands: Springer.
38. Cox N, Messinger J. 2013 Reflections on substrate water and dioxygen formation. *Biochim. Biophys. Acta* **1827**, 1020–1030. (doi:10.1016/j.bbabio.2013.01.013)
39. Becker K, Cormann KU, Nowaczyk MM. 2011 Assembly of the water-oxidizing complex in photosystem II. *J. Photochem. Photobiol. B* **104**, 204–211. (doi:10.1016/j.jphotobiol.2011.02.005)
40. Dasgupta J, Ananyev GM, Dismukes GC. 2008 Photoassembly of the water-oxidizing complex in photosystem II. *Coordin. Chem. Rev.* **252**, 347–360. (doi:10.1016/j.ccr.2007.08.022)
41. Suga M *et al*. 2015 Native structure of photosystem II at 1.95 Å resolution viewed by femtosecond X-ray pulses. *Nature* **517**, 99–103. (doi:10.1038/nature13991)
42. Dau H, Haumann M. 2008 The manganese complex of photosystem II in its reaction cycle—basic framework and possible realization at the atomic level. *Coordin. Chem. Rev.* **252**, 273–295. (doi:10.1016/j.ccr.2007.09.001)
43. Glöckner C, Kern J, Broser M, Zouni A, Yachandra V, Yano J. 2013 Structural changes of the oxygen-evolving complex in photosystem II during the catalytic cycle. *J. Biol. Chem.* **288**, 22 607–22 620. (doi:10.1074/jbc.M113.476622)
44. Haumann M *et al*. 2005 Structural and oxidation state changes of the photosystem II manganese complex in four transitions of the water oxidation cycle ($S_0 \rightarrow S_1$, $S_1 \rightarrow S_2$, $S_2 \rightarrow S_3$, and $S_{3,4} \rightarrow S_0$) characterized by X-ray absorption spectroscopy at 20 K and room temperature. *Biochemistry* **44**, 1894–1908. (doi:10.1021/bi048697e)
45. Pushkar YL, Yano J, Sauer K, Boussac A, Yachandra VK. 2008 Structural changes in the Mn_4Ca cluster and the mechanism of photosynthetic water splitting. *Proc. Natl Acad. Sci. USA* **105**, 1879–1884. (doi:10.1073/pnas.0707092105)
46. Yano J *et al*. 2006 Where water is oxidized to dioxygen: structure of the photosynthetic Mn_4Ca cluster. *Science* **314**, 821–825. (doi:10.1126/science.1128186)
47. Galstyan A, Robertazzi A, Knapp EW. 2012 Oxygen-evolving Mn cluster in photosystem II: the protonation pattern and oxidation state in the high-resolution crystal structure. *J. Am. Chem. Soc.* **134**, 7442–7449. (doi:10.1021/ja300254n)
48. Luber S, Rivalta I, Umena Y, Kawakami K, Shen J-R, Kamiya N, Brudvig GW, Batista VS. 2011 S1-State model of the O_2-evolving complex of photosystem II. *Biochemistry* **50**, 6308–6311. (doi:10.1021/bi200681q)
49. Grundmeier A, Dau H. 2012 Structural models of the manganese complex of photosystem II and mechanistic implications. *Biochim. Biophys. Acta* **1817**, 88–105. (doi:10.1016/j.bbabio.2011.07.004)
50. Zimmermann JL, Rutherford AW. 1984 EPR studies of the oxygen-evolving enzyme of photosystem II. *Biochim. Biophys. Acta* **767**, 160–167. (doi:10.1016/0005-2728(84)90091-4)
51. Boussac A, Girerd J-J, Rutherford AW. 1996 Conversion of the spin state of the manganese complex in photosystem II induced by near-infrared light. *Biochemistry* **35**, 6984–6989. (doi:10.1021/bi960636w)
52. Pantazis DA, Ames W, Cox N, Lubitz W, Neese F. 2012 Two interconvertible structures that explain the spectroscopic properties of the oxygen-evolving complex of photosystem II in the S2 state. *Angew. Chem. Int. Ed.* **51**, 9935–9940. (doi:10.1002/anie.201204705)
53. Bovi D, Narzi D, Guidoni L. 2013 The S_2 state of the oxygen-evolving complex of photosystem II explored by QM/MM dynamics: spin surfaces and metastable states suggest a reaction path towards the S_3 state. *Angew. Chem. Int. Ed.* **52**, 11 744–11 749. (doi:10.1002/anie.201306667)
54. Isobe H, Shoji M, Yamanaka S, Umena Y, Kawakami K, Kamiya N, Shen JR, Yamaguchi K. 2012 Theoretical illumination of water-inserted structures of the $CaMn_4O_5$ cluster in the S_2 and S_3 states of oxygen-evolving complex of photosystem II: full geometry optimizations by B3LYP hybrid density functional. *Dalton Trans.* **41**, 13 727–13 740. (doi:10.1039/c2dt31420g)
55. Krewald V, Retegan M, Cox N, Messinger J, Lubitz W, DeBeer S, Neese F, Pantazis D. 2015 Metal oxidation states in biological water splitting. *Chem. Sci.* **6**, 1676–1695. (doi:10.1039/C4SC03720K)
56. Cox N, Retegan M, Neese F, Pantazis DA, Boussac A, Lubitz W. 2014 Electronic structure of the oxygen-evolving complex in photosystem II prior to O-O bond formation. *Science* **345**, 804–808. (doi:10.1126/science.1254910)
57. Lohmiller T *et al*. 2014 Structure, ligands and substrate coordination of the oxygen-evolving complex of photosystem II in the S_2 state: a combined EPR and DFT study. *Phys. Chem. Chem. Phys.* **16**, 11 877–11 892. (doi:10.1039/c3cp55017f)
58. Rapatskiy L *et al*. 2012 Detection of the water-binding sites of the oxygen-evolving complex of photosystem II using W-band ^{17}O electron–electron double resonance-detected NMR spectroscopy. *J. Am. Chem. Soc.* **134**, 16 619–16 634. (doi:10.1021/ja3053267)
59. Siegbahn PEM. 2013 Water oxidation mechanism in photosystem II, including oxidations, proton release pathways, O–O bond formation and O_2 release. *Biochim. Biophys. Acta* **1827**, 1003–1019. (doi:10.1016/j.bbabio.2012.10.006)
60. Noguchi T. 2008 FTIR detection of water reactions in the oxygen-evolving centre of photosystem II. *Phil. Trans. R. Soc. B* **363**, 1189–1195. (doi:10.1098/rstb.2007.2214)
61. Dau H, Liebisch P, Haumann M. 2005 The manganese complex of oxygenic photosynthesis conversion of five coordinated Mn(III) to six coordinated Mn(IV) in the S_2–S_3 transition is implied by XANES simulations. *Phys. Scripta* **2005**, 844. (doi:10.1238/Physica.Topical.115a00844)
62. Messinger J, Robblee JH, Yu WO, Sauer K, Yachandra VK, Klein MP. 1997 The S_0 state of the oxygen-evolving complex in photosystem II is paramagnetic: detection of an EPR multiline signal. *J. Am. Chem. Soc.* **119**, 11 349–11 350. (doi:10.1021/ja972696a)
63. Yamauchi T, Mino H, Matsukawa T, Kawamori A, Ono T. 1997 Parallel polarization electron paramagnetic resonance studies of the S_1-state manganese cluster in the photosynthetic oxygen-evolving system. *Biochemistry* **36**, 7520–7526. (doi:10.1021/bi962791g)
64. Messinger J, Badger M, Wydrzynski T. 1995 Detection of one slowly exchanging substrate water molecule in the S_3 state of photosystem II. *Proc. Natl Acad. Sci. USA* **92**, 3209–3213. (doi:10.1073/pnas.92.8.3209)
65. Hillier W, Wydrzynski T. 2000 The affinities for the two substrate water binding sites in the O_2 evolving complex of photosystem II vary independently during S-state turnover. *Biochemistry* **39**, 4399–4405. (doi:10.1021/bi992318d)

66. Hillier W, Wydrzynski T. 2004 Substrate water interactions within the photosystem II oxygen evolving complex. *Phys. Chem. Chem. Phys.* **6**, 4882–4889. (doi:10.1039/b407269c)
67. Hillier W, Wydrzynski T. 2008 ^{18}O-Water exchange in photosystem II: substrate binding and intermediates of the water splitting cycle. *Coordin. Chem. Rev.* **252**, 306–317. (doi:10.1016/j.ccr.2007.09.004)
68. Cox N, Lubitz W, Savitsky A. 2013 W-band ELDOR-detected NMR (EDNMR) spectroscopy as a versatile technique for the characterisation of transition metal–ligand interactions. *Mol. Phys.* **111**, 2788–2808. (doi:10.1080/00268976.2013.830783)
69. Beck WF, De Paula JC, Brudvig GW. 1986 Ammonia binds to the manganese site of the oxygen-evolving complex of photosystem II in the S2 state. *J. Am. Chem. Soc.* **108**, 4018–4022. (doi:10.1021/ja00274a027)
70. Britt RD, Zimmermann JL, Sauer K, Klein MP. 1989 Ammonia binds to the catalytic manganese of the oxygen-evolving complex of photosystem II. Evidence by electron spin-echo envelope modulation spectroscopy. *J. Am. Chem. Soc.* **111**, 3522–3532. (doi:10.1021/ja00192a006)
71. Pérez Navarro M *et al*. 2013 Ammonia binding to the oxygen-evolving complex of photosystem II identifies the solvent-exchangeable oxygen bridge (μ-oxo) of the manganese tetramer. *Proc. Natl Acad. Sci. USA* **110**, 15 561–15 566. (doi:10.1073/pnas.1304334110)
72. Schraut J, Kaupp M. 2014 On ammonia binding to the oxygen-evolving complex of photosystem II: a quantum chemical study. *Chem. Eur. J.* **20**, 7300–7308. (doi:10.1002/chem.201304464)
73. Hou L-H, Wu C-M, Huang H-H, Chu H-A. 2011 Effects of ammonia on the structure of the oxygen-evolving complex in photosystem II as revealed by light-induced FTIR difference spectroscopy. *Biochemistry* **50**, 9248–9254. (doi:10.1021/bi200943q)
74. Hendry G, Wydrzynski T. 2003 ^{18}O isotope exchange measurements reveal that calcium is involved in the binding of one substrate-water molecule to the oxygen-evolving complex in photosystem II. *Biochemistry* **42**, 6209–6217. (doi:10.1021/bi034279i)
75. Nilsson H, Krupnik T, Kargul J, Messinger J. 2014 Substrate water exchange in photosystem II core complexes of the extremophilic red alga *Cyanidioschyzon merolae*. *Biochim. Biophys. Acta* **1837**, 1257–1262. (doi:10.1016/j.bbabio.2014.04.001)
76. Narzi D, Bovi D, Guidoni L. 2014 Pathway for Mn-cluster oxidation by tyrosine-Z in the S2 state of photosystem II. *Proc. Natl Acad. Sci. USA* **111**, 8723–8728. (doi:10.1073/pnas.1401719111)
77. Boussac A, Rutherford AW. 1988 Nature of the inhibition of the oxygen-evolving enzyme of photosystem II induced by sodium chloride washing and reversed by the addition of calcium(2^+) or strontium(2^+). *Biochemistry* **27**, 3476–3483. (doi:10.1021/bi00409a052)
78. Boussac A, Zimmermann JL, Rutherford AW. 1989 EPR signals from modified charge accumulation states of the oxygen-evolving enzyme in calcium-deficient photosystem II. *Biochemistry* **28**, 8984–8989. (doi:10.1021/bi00449a005)
79. Sivaraja M, Tso J, Dismukes GC. 1989 A calcium-specific site influences the structure and activity of the manganese cluster responsible for photosynthetic water oxidation. *Biochemistry* **28**, 9459–9464. (doi:10.1021/bi00450a032)
80. Siegbahn PEM. 2009 Structures and energetics for O_2 formation in photosystem II. *Acc. Chem. Res.* **42**, 1871–1880. (doi:10.1021/ar900117k)
81. Rutherford AW. 1989 Photosystem II, the water-splitting enzyme. *Trends Biochem. Sci.* **14**, 227–232. (doi:10.1016/0968-0004(89)90032-7)
82. Wiechen M, Berends H-M, Kurz P. 2012 Water oxidation catalysed by manganese compounds: from complexes to 'biomimetic rocks'. *Dalton Trans.* **41**, 21–31. (doi:10.1039/C1DT11537E)
83. Tsui EY, Tran R, Yano J, Agapie T. 2013 Redox-inactive metals modulate the reduction potential in heterometallic manganese–oxido clusters. *Nat. Chem.* **5**, 293–299. (doi:10.1038/nchem.1578)
84. Wiechen M, Zaharieva I, Dau H, Kurz P. 2012 Layered manganese oxides for water-oxidation: alkaline earth cations influence catalytic activity in a photosystem II-like fashion. *Chem. Sci.* **3**, 2330–2339. (doi:10.1039/c2sc20226c)
85. Lassalle-Kaiser B, Hureau C, Pantazis DA, Pushkar Y, Guillot R, Yachandra VK, Yano J, Neese F, Anxolabéhère-Mallart E. 2010 Activation of a water molecule using a mononuclear Mn complex: from Mn-aquo, to Mn-hydroxo, to Mn-oxyl via charge compensation. *Energy Environ. Sci.* **3**, 924–938. (doi:10.1039/b926990h)
86. Sameera WMC, McKenzie CJ, McGrady JE. 2011 On the mechanism of water oxidation by a bimetallic manganese catalyst: a density functional study. *Dalton Trans*. **40**, 3859–3870. (doi:10.1039/c0dt01362e)
87. Yamaguchi K, Takahara Y, Fueno T. 1986 Ab-initio molecular orbital studies of structure and reactivity of transition metal oxo compounds. In *Applied quantum chemistry* (eds VH Smith, HF Schaefer, K Morokuma), pp. 155–184. Boston, MA: Reidel.
88. Siegbahn PEM, Crabtree RH. 1998 Manganese oxyl radical intermediates and O—O bond formation in photosynthetic oxygen evolution and a proposed role for the calcium cofactor in photosystem II. *J. Am. Chem. Soc.* **121**, 117–127. (doi:10.1021/ja982290d)
89. Kanady JS, Tsui EY, Day MW, Agapie T. 2011 A synthetic model of the Mn_3Ca subsite of the oxygen-evolving complex in photosystem II. *Science* **333**, 733–736. (doi:10.1126/science.1206036)
90. Mukherjee S *et al*. 2012 Synthetic model of the asymmetric [Mn_3CaO_4] cubane core of the oxygen-evolving complex of photosystem II. *Proc. Natl Acad. Sci. USA* **109**, 2257–2262. (doi:10.1073/pnas.1115290109)
91. Krewald V, Neese F, Pantazis DA. 2013 On the magnetic and spectroscopic properties of high-valent Mn_3CaO_4 cubanes as structural units of natural and artificial water-oxidizing catalysts. *J. Am. Chem. Soc.* **135**, 5726–5739. (doi:10.1021/ja312552f)
92. Najafpour MM, Ehrenberg T, Wiechen M, Kurz P. 2010 Calcium manganese(III) oxides ($CaMn_2O_4 \cdot xH_2O$) as biomimetic oxygen-evolving catalysts. *Angew. Chem. Int. Ed.* **49**, 2233–2237. (doi:10.1002/anie.200906745)
93. Zaharieva I, Najafpour MM, Wiechen M, Haumann M, Kurz P, Dau H. 2011 Synthetic manganese–calcium oxides mimic the water-oxidizing complex of photosynthesis functionally and structurally. *Energy Environ. Sci.* **4**, 2400–2408. (doi:10.1039/c0ee00815j)